QoE and Cost-Aware Resource and Interference Management in Aerial-Terrestrial Networks for Vehicular Applications

QoE and Cost-Aware Resource and Interference Management in Aerial-Terrestrial Networks for Vehicular Applications

Danila Ferretti, Silvia Mignardi, Riccardo Marini, Roberto Verdone, Chiara Buratti

***Abstract*—In this paper, we address the deployment of Unmanned Aerial Vehicles (UAVs) as Unmanned Aerial Base Stations (UABSs) which cooperate with Macro Base Stations (MBSs) in an urban environment to serve vehicles, denoted as Ground User Equipments (GUEs), implementing vehicle-to-everything (V2X) services. As vehicles perform extended sensing, exchanging data with nearby GUEs through UAVs and MBSs links, we propose an Integer Linear Programming (ILP) model that jointly optimizes radio resources allocation and beamforming, while accounting for vehicular application requirements, backhaul capacity limits and interference between GUE-UABS and GUE-MBS links. The model allows also to find a trade-off between benefits and cost of UABSs activation. Two system architectures are considered: a distributed model, where MBSs independently run the Radio Resource Management (RRM) algorithm sharing information with each other, and a centralized model, where MBSs send information to the network core, where the optimization algorithm runs. The study investigates interference through two resource allocation approaches, considering splitting and sharing of resources among UABSs and MBSs. Numerical evaluations demonstrate the effectiveness of using UABSs to improve the Quality of Experience (QoE) of GUEs. We also compare the two architectures, considering both resource pool assignments, and highlighting the impact of varying UABSs parameters and activation costs.**

***Index Terms*—UAV, 5G, Joint RRM, Uplink Interference, Beamforming, Vehicular Wireless Networks.**

I. Introduction

THE rising and relevance of Unmanned Aerial Vehicles (UAVs) in civil applications, like delivery, video monitoring, photogrammetry and others, lead to increased use of professional drones even in urban environments. With the new technology advancements, professional UAVs will be safer, will carry heavier payloads, and will last for a longer flight time. For these reasons, we can predict a huge increase in the use of professional UAVs in urban environments. In addition, while UAVs fly over a city to perform their primary mission (such as monitoring via on-board cameras), we envision they can also carry small Base Station (BS) equipment so that they can be activated as Unmanned Aerial BSs (UABSs) to provide wireless communication services when needed. In such cases, UABSs will support the radio terrestrial infrastructure to serve ground users seeking a network connection.

In this work we consider a scenario where terrestrial Macro BSs (MBSs) and multiple UAVs, following a predefined path, are deployed in an urban scenario, to serve vehicles moving in the area, hereafter denoted as *ground user equipments (GUEs)*. UAVs can activate the UABSs on board to help the terrestrial network when needed. Indeed, we assume the activation of the UABS has a given cost to be accounted for, making convenient the identification of the best time when the activation should be performed. Vehicles perform an extended sensing application, according to which they need to exchange huge amounts of data with other vehicles nearby, either via a MBS or a UABS. Through sensors mounted onboard, each vehicle, for a given amount of time, gathers data about its surroundings to be sent in uplink, then the network will process the data and send it back to vehicles. In the following we will focus on the uplink traffic and we will denote as *demand* the amount of data to be transmitted by each GUEs. In particular, the proposed model aims at maximizing the Quality of Experience (QoE) of users, which are able to upload their demand for a continuous amount of time. By considering the scenario and application described above, we propose an Integer Linear Program (ILP) that jointly addresses vehicular applications' requirements, UABS backhaul capacity and radio resource management (RRM), trying to minimize interference between GUE-UABS and GUE-MBS links. The RRM is performed based on beamforming at the UABSs and GUEs sides so that beam activation is optimized jointly with time-frequency resource allocation. In addition, the model allows to trade-off between the benefits of activating UABSs and the cost of such activation. The analysis has been conducted by considering two possible system architectures: i) a distributed model, where MBSs run the RRM algorithm separately, sharing environment information with each other and managing signalling with a subset of UABSs; ii) a centralized model, where MBSs send their information to the network core, which is in charge

(Corresponding author: Danila Ferretti.)

Danila Ferretti is with the National Laboratory of Wireless Communications of CNIT (WiLab, CNIT), Italy and the Department of Information Engineering, Electronics and Telecommunications, La Sapienza, University of Rome, Italy (e-mail: danila.ferretti@wilab.cnit.it).

Silvia Mignardi is with the Department of Electrical Energy and Information Engineering, University of Bologna, Italy (e-mail: silvia.mignardi92@gmail.com).

Riccardo Marini is with the National Laboratory of Wireless Communications of CNIT (WiLab, CNIT), Italy (e-mail: riccardo.marini@wilab.cnit.it).

Roberto Verdone is with the Department of Electrical Energy and Information Engineering, University of Bologna, Italy and with the National Laboratory of Wireless Communications of CNIT (WiLab, CNIT), Italy (e-mail: roberto.verdone@unibo.it).

Chiara Buratti is with the Department of Electrical Energy and Information Engineering, University of Bologna, Italy and with the National Laboratory of Wireless Communications of CNIT (WiLab, CNIT), Italy (e-mail: c.buratti@unibo.it).

of running the RRM algorithm. Furthermore, we investigate the impact of interference by analyzing two different resource set allocations: resource split and resource sharing. In the former, two BS will interfere with each other only if they are both terrestrial or both aerial since all MBSs exploit the same pool of resource units (RUs) (the same applies to UABSs), and an orthogonal one with UABSs, whereas in the latter MBSs and UABSs share the entire resource pool, and thus, the interference must always be taken into account. Numerical evaluations show how the adaptive behaviour of UAVs helps the terrestrial infrastructure to improve the performance, by comparing the two architectures considered (distributed and centralized), considering both split and shared resource pool assignment, with a benchmark case where no UABSs are deployed in the scenario. We also show how changing UABS-related parameters, such as its footprint, the grid of beams or the cost of the UABSs activation, impact the results, investigating the consequent trade-offs.

The rest of this paper is organized as follows. First, Section II introduces the literature state of the art. The network model is described in Section III, including the reference scenario and application requirements, the two alternative system architectures and the UAVs trajectory. The RRM problem formulation and implementation for the different architectures follow in Section IV and Section V, respectively. Numerical results are discussed in Section VI and Section VII concludes the paper.

II. Literature Overview

The application of UAVs in mobile networks has been extensively investigated in the recent scientific literature. One of the widely explored topics is RRM when UAVs support the terrestrial network and very often this topic is jointly analyzed with other aspects, such as beamforming, backhaul capacity limits, etc. Table I classifies a sample of recent papers, reporting whether they discuss or account for the following aspects: multi-UAVs scenario, interference management, beamforming, backhaul and QoE.

Authors in [1] investigate spectrum efficiency and optimize served users to separate the optimization problem into two sub-problems, related to user association and optimal placement. Authors in [2] propose two heuristic and scalable solutions for resource-aware UAV flight planning. Among studies that consider interference but not beamforming, [3] proposes a hybrid algorithm to determine optimal UAV placement in a traffic offloading scenario, aiming to maximize system capacity. In [4] and [5], authors focus on maximizing energy efficiency through power allocation optimization. Furthermore, [6] addresses the optimal 3D-trajectory design and UAV resource allocation. However, these RRM problems neglect the optimization of backhaul connections, which are crucial for UAV-aided architectures. [7]–[10] investigate multi-UAV scenarios: in [7], UAVs deliver critical data in vehicular networks during emergencies; [8] addresses UAV deployment and resource allocation; [9] analyzes user association and caching, while [10] focuses on network throughput with RRM and backhaul. However, these studies do not consider beamforming and the challenges associated with unpredictable user movement. In [11], authors explore the same topic as [7] but focus on single-UAV applications. [12] and [13] analyze energy consumption as a cost metric, while [13] specifically addresses jamming policies to maximize energy efficiency. However, these studies do not prioritize investigating end users' QoE. In our work, we define user satisfaction based on consecutive time slots service. The topic is investigated in [14], but in a single-UAV scenario with no interference or backhaul considerations.

In [15]–[17] trajectory and RRM are optimized without considering interference. For instance, [15] focuses on a caching-based UAV trajectory. Studies by [16], [17] specifically explore a multi-UAV scenario, with the former aiming to maximize the number of users while satisfying their data transmission demand and the latter focusing on optimizing the energy consumption of UAVs. In contrast, our work differs as we optimize link selection taking interference into account. Among studies addressing interference, [18] explores weighted power assignment to minimize UAV energy consumption. [19] optimizes subchannel assignment and user association for fair resource sharing among GUEs. [20] focuses on energy harvesting, while [21] jointly considers user scheduling and power allocation for energy efficiency. Backhaul is considered only in [22] with predictable user movement. Lastly, [23] maximizes the sum rate while addressing self-interference cancellation. Importantly, none of these works incorporates QoE or beamforming considerations. [24] only consider beams from MBSs, while [25] and [26] specifically investigate UAV beamforming. While [24] focuses on RRM strategies in caching networks, [25] optimizes UAV trajectory and GUE transmission power. These do not consider the interference issue, while our work extensively investigates it.

TABLE I
Reference Papers

Ref.	Multi-UAV	Int.	Beamforming	Backhaul	QoE
[1]	√	√	√ (MBS)	√	
[2]	√				
[3]	√	√			
[4]	√	√			√
[5]	√	√			
[6]		√			
[7]	√				√
[8]	√				
[9]	√	√			
[10]	√	√		√	
[11]		√			
[12]		√			
[13]	√	√	√		
[14]					√
[15]				√	
[16]	√				√
[17]	√				
[18]	√	√			
[19]	√	√			
[20]		√			
[21]		√			
[22]		√		√	
[23]	√	√			
[24]	√		√ (MBS)		
[25]			√		
[26]	√		√	√	√
▼	√	√	√	√	√

Ref.: reference work; Int.: interference; ▼: this work.

Table I shows whether the topics discussed are investigated in the reference works (marked with a $\surd$).

To summarize, in contrast with the scientific literature, this work's contributions are the following:

- We consider a complex urban vehicular scenario, where GUEs are characterized by a high degree of dynamism, which makes the RRM process quite complex to handle;
- We analyze an application where UAVs are deployed to perform a predefined mission (different from communication) and may activate BSs on board when it is convenient;
- Since a portion of the resource pool is allocated to perform signalling, the backhaul issue between UABSs and MBSs is investigated;
- QoE of final users is optimized, to ensure that the vehicles are served for several consecutive slots;
- Beamforming is accounted for when dealing with communication links between UABSs and GUEs.

Moreover, extending our work in [26], we investigated:

- Two possible network infrastructures (distributed and centralized) to analyze the trade-off between signalling complexity and efficiency.
- Uplink links that interfere with each other, both among MBSs and UABSs.
- A cost of activation of UAVs as UABSs. In this way, the algorithm has to optimize the number of satisfied users, given that turning on each UABS will negatively impact the objective function.

III. System Model

A. Reference Scenario and Application

We consider an urban scenario with the elements depicted in Figure 1. A set $\mathcal{A}$ of UAVs is flying above the area at a constant altitude, h, from the ground. We assume that each UAV is dedicated to a predefined mission, following the predefined trajectory described in [26] and denoted as Paparazzi-scan. At the same time, each UAV has radio-frequency equipment on board (i.e., acts as UABS). Fixed on the ground there are terrestrial MBSs, being part of a set $\mathcal{M}$ and GUEs g, belonging to the set $\mathcal{G}$, move in the environment.

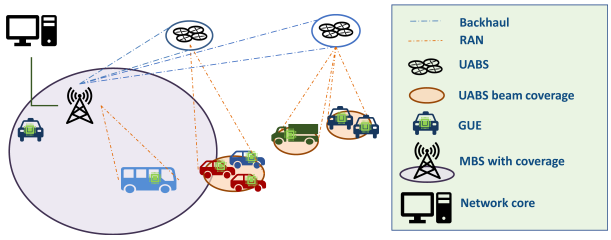

Fig. 1. Network components and architecture.

MBSs have wired connections with the network core, therefore, we assume this link to be robust and to have sufficient capacity to forward signalling and content. On the opposite, UABSs have to maintain a wireless communication link with MBSs to receive the necessary command and control signalling and to reach the network core. This backhaul link is subject to RRM optimization.

From the users' side, we consider an extended sensing application, according to which each GUE wants to exchange data gathered through local sensors or video with the network and other GUEs nearby. By exchanging vehicle-to-anything (V2X) messages [27], GUE can enhance the perception of their surroundings beyond what their own sensors can detect. As sensor data should be sent from GUEs to the network for their collection, the traffic requirements are particularly challenging for the uplink (UL) communication [28]. The traffic demand, D_g, for the GUE $g \in \mathcal{G}$ depends on the degree of automation considered, with a data rate ranging from 1 to 1000 Mbps [28]. The mobility of GUEs and UABSs leads to a dynamic scenario, considered by updating the traffic demand of GUEs with a time granularity[2] of $\Delta t = 100$ ms.

We define a GUE, g, as *served* in a given interval, Δt, if it is able to upload its demand D_g. Then, to account for vehicles' QoE, we define a GUE, g, as *satisfied* if it is served for at least $\hat{N}_\mathrm{s}$ time intervals within a given time window, $T_w = N_\mathrm{w}\,\Delta t$ (being $\hat{N}_\mathrm{s}$ a given percentage of N_w). The QoE requirement, $\hat{N}_s$, is determined by the time the vehicle may take to execute a manoeuvre (e.g., turn at crossroads, enter/exit roundabouts, stops, and so on). Example values are reported in [31], considering the average values of vehicles' speed and communication range in specific use cases. The percentage of users *satisfied*, $P_g^{(sat)}$, is used as a performance metric.

B. UAVs Trajectory

As previously mentioned, we assume UAVs in the scenario have predefined missions (other than communication) constraining them flying on an already determined trajectory. Possible UAVs' tasks might be video-monitoring an area or collecting sensor data scattered all over the scenario. A suitable trajectory for such missions is a Paparazzi-scan, which shapes a serpentine that scans the entire area [32]. An example is pictured in Figure 2, while Figure 3 shows the real-world scenario in which we run the proposed model, specifically in the historic center of Bologna.

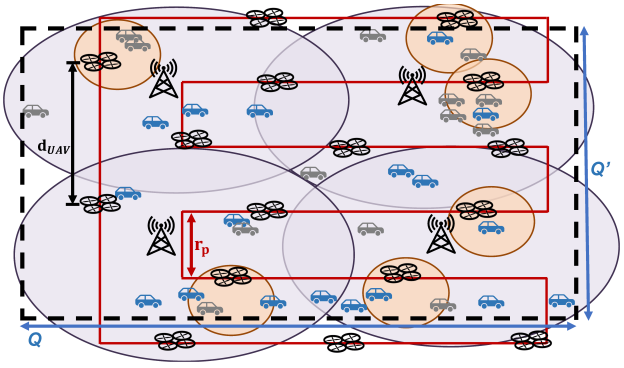

Fig. 2. Example where UAVs follow a Paparazzi-scan trajectory to accomplish a predetermined task.

To model the UAV movement, the scan serpentine is completely defined by the area side and a parameter introduced

[2]Note that 100 ms is the packet generation interval for many types of V2X including Cooperative Awareness Message (CAM) and Collective Perception Message (CPM) [29], [30]

on purpose, which we name Paparazzi-scan sensing radius, r_p. The value of $2\,r_p$ defines the serpentine width, while height and length are respectively denoted as Q and Q'. The r_p choice depends on the UAVs potential coverage; its definition allows UAVs to eventually cover the entire service area for a number of UAVs, N_{uav}. Each new UAV enters the scan trajectory every t_p and d_{UAV} represents the distance between each UAV. Please note that the model presented hereafter works independently from the UAV trajectory, and it can be re-applied for any given UAV path.

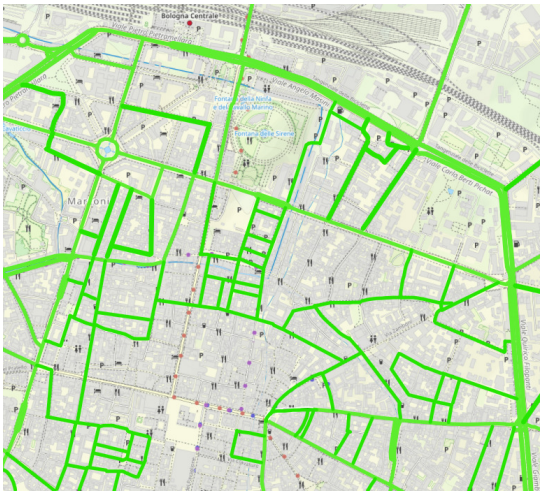

Fig. 3. Real-world scenario tested in simulations, located in the historic center of Bologna.

C. Network Architectures

The architecture considered is reported in Figure 4; the GUEs are connected either to MBSs or UABSs via an access wireless link and the aerial BSs are connected to the terrestrial BSs via a backhaul wireless link. Moreover, MBSs can communicate with each other and with the network core through a wireline IP link. Based on this block diagram, we consider four cases based on the architecture and resource pool applied:

1) Case I: Distributed Architecture with Resource Split: The RRM runs at each MBS separately, handling a predefined subset of GUEs and UABSs in the scenario, which are those receiving the largest receive power from the MBS. Moreover, since interference is taken into account, MBSs share non-real-time, worst-case scenario information on the level of interference coming from the other subsets (i.e., GUEs and UABSs connected to other MBSs). The exchange happens through the wireline Internet Protocol (IP) link. The resource pool is halved: one half is used by MBSs to serve GUEs, the orthogonal half is used by UABSs. Therefore, MBSs interfere with other MBSs, and the same applies to UABSs, but MBSs and UABSs do not interfere with each other. This concept is further explained in Table II under subsection III-G.

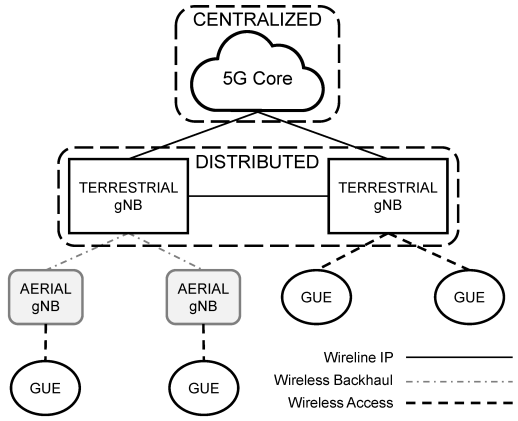

Fig. 4. Network Architecture: distributed or centralized.

2) Case II: Distributed Architecture with Resource Sharing: The RRM runs in the same way as in Case I, but when the resources are shared, all BSs share the entire resource pool, whether the GUE is served by a MBS or a UABS.

3) Case III: Centralized Architecture with Resource Split: The RRM runs at the network core and takes all decisions related to the area of interest, meaning that MBSs send information to the core network (i.e., a controller) based on all potential links present in the area. The interference information is real-time and not based on the worst-case scenario. The resource pool is halved in the same way as it is for Case I.

4) Case IV: Centralized Architecture with Resource Split: The RRM runs in the same way as in Case III, but the resource pool is shared as in Case II.

D. Channel Model

The channel model follows the Urban Macro (UMa) channel described in the 3GPP TR 38.901 [33]. The considered model provides different channel descriptions for line of sight (LoS) and Non-LoS (NLoS) conditions through the exploitation of the parameter ρ_L which is the probability of being in LoS condition that depends on the distance between the considered GUEs g, regarded as *transmitters*, and the UABS/MBSs, the *receivers*, and on the height of g, h_g. The path loss variation due to shadowing can be described through a log-normal distribution zero-mean and with a standard deviation $\sigma_{\text{LoS}} = 4$ dB and $\sigma_{\text{NLoS}} = 6$ dB for LoS and NLoS respectively. The propagation loss determines the robustness of a link, and allows the computation of the relevant metrics of Signal-to-Noise ratio (SNR) and Signal-to-Interference-plus-Noise ratio (SINR), taking into account both noise and interference [26]. In particular, we consider the situation in which the channel fluctuations do not change significantly, i) in the time interval in which RRM takes place when the environment dynamism cannot be appreciated and ii) among different frequency offsets within the predefined bandwidth, B. Then, we can compute the SNR, γ, and the SINR, $\gamma^{(I)}$, (in linear scale) as

$$\gamma = \frac{P_{\text{rx}}}{P_{\text{noise}}}, \tag{1}$$

$$\gamma^{(I)} = \frac{P_{\text{rx}}}{P_{\text{noise}} + \sum_{i=1}^{N_{int}} P_{\text{rx,i}}}, \tag{2}$$

where P_{rx} is referring to a generic useful link and indicates the receiver power, P_{noise} denotes the noise power, and $P_{\text{rx,i}}$ indicates the interfering power from interferer i supposing N_{int} total interferers are present. Consequently, the data rate a single link can achieve depends on the SNR or SINR values

computed through the Shannon capacity formulas. Then, a link can be established if the SNR and the SINR are above a given threshold, γ_{th} and γ^I_{th}, respectively. If this is the case, the data rate can be computed only on the SNR (if it is noise-limited) or on the SINR. Thus, given a bandwidth portion, B_{ch}, we have:

$$r = B_{\text{ch}} \log_2(1+\gamma). \tag{3}$$

$$r^{(I)} = B_{\text{ch}} \log_2(1+\gamma^{(I)}). \tag{4}$$

E. Radio Resource Unit

Regarding RUs, they encompass time, frequency, and space dimensions for facilitating network communication. The time-frequency aspect aligns with the 3rd Generation Partnership Project (3GPP) fifth-generation (5G) standard numerology [34]. A set of time-frequency radio resources comprises resource blocks (RBs), with each RB containing 12 consecutive subcarriers transmitting an orthogonal frequency-division multiplexing (OFDM) signal. Subcarriers cover the frequency axis with a spacing of Δf. Time-wise, RB boundaries align with time slots lasting T_{slot}, accommodating 14 OFDM symbols based on the chosen Δf. The selected bandwidth value, B, determines the available RBs count, denoted as W, formalized as:

$$W = B_{\text{ch}} \cdot (\Delta t / T_{\text{slot}}) \tag{5}$$

where $B_{\text{ch}} = \frac{B}{12\Delta f}$.

Additionally, beamforming defines the spatial aspect using multiple *covering beams*. Regarding UABS beam modeling, we define $\phi^{(u)}$ as the vertical field of view and $\Phi^{(u)}$ as the corresponding solid angle. By relating them through $\Phi^{(u)} = 2\pi(1-\cos(\phi^{(u)}/2))$, we can approximate the solid angle of an individual beam as $\Phi^{(u)}_{\text{beam}} \approx \Phi^{(u)}/N_{\text{beam}}$. Finally, the receiving gain of UABS can be expressed as follow [35]:

$$G_{\text{beam}} = \frac{41000}{\left(\Phi^{(u)}_{\text{beam}} \frac{360}{2\pi}\right)^2}. \tag{6}$$

We assume an ideal radiation pattern with gain G_{beam} within $\phi^{(u)}_{\text{beam}}$ and 0 dB outside. GUEs outside the beam are not considered connected to the UABS, representing a worst-case connectivity scenario. With fully digital or hybrid beamforming, the number of available beams K depends on the UAV's transceiver chains. Depending on the beam pattern, RUs can be orthogonal or not. If a source's beam covers unintended receivers, interference occurs on the same time-frequency RBs. Each MBS can activate all ground footprint beams, while UABSs are limited to N_{beam} out of K beams to manage payload and energy consumption. Therefore, optimizing beam selection based on current GUE demand becomes crucial. Each source utilizes specific beams to cover different users, denoting a RU as one RB over a covering beam. The granularity of the allocation is based on a Radio Resource Block, which is composed of a slot, of duration T_{slot}, a bandwidth, B_{ch}, and a portion of space equal to $\Phi^{(u)}_{\text{beam}}$. Numerical parameters are reported in Table III.

F. Link Definition

Given the definition of RU, we now observe the different links that could be established in the network, being:

- UABS-MBS link: the wireless backhaul forwards all traffic handled by UABSs to the MBSs. We assign dedicated resources to backhaul links, not shared with access links, because of the bottleneck represented by these links. Clearly, because of the scenario dynamicity, the set of RUs given to backhaul might change over time.
- GUE-MBS link: reuse of RBs in the space dimension is not applied, since, given the wide area to cover, MBSs' beams might create overlapping footprints on the ground, resulting in interference.
- GUE-UABS link: reuse of RBs in the space dimension is applied, since UABSs fly at heights above those of the MBSs (hundreds of meters against 25-30 meters), and each beam's resulting coverage spot on the 2D ground plane is smaller and better distinguishable from others.

G. Interference Analysis

Depending on RUs assignment, the system may need to counteract interference problems. The total number of RBs at the disposal of MBSs and UABSs depends on the resource allocation strategy used: for the *resource splitting* case, we assume MBSs and UABSs use an orthogonal subset of the available RBs, $W/2$ each, whereas, when *resource sharing* is exploited, all BSs share the same set of RBs, W. Then, accounting for the fact that reuse of RBs can be applied for UABSs, but not for MBSs, the total amount of RUs available will be W^*_m equal to $W/2$ (or W) for MBSs and W^*_a equal to $W/2 \cdot K$ (or $W \cdot K$) for UABSs. Table II summarizes the interfering links for the different approaches. In the case of resource splitting the system suffers from interference only on GUE-BS links if the interfering BS share the same typology (aerial or terrestrial). In the resource sharing case, the scheduler shares the same set of resources in the GUE-MBS and GUE-UABS links to improve the spectrum efficiency, therefore interference is always present.

TABLE II
INTERFERING LINKS

		UL interfering link		
	Links	GUE - UABS	GUE - MBS	UABS - MBS
UL useful links	GUE - UABS	√	△	×
	GUE - MBS	△	√	×
	UABS - MBS	×	×	×

√: interfering; ×: non-interfering; △: only with shared RUs.

As far as the treatment of interference in the two architectures is concerned, in the distributed case, each MBS is in charge of assigning RUs to UABSs and GUEs, so it is able to predict interference on its GUE and UABS-GUE links, but it cannot evaluate in advance the possible interference coming from links established with other MBSs. On the contrary, the centralized architecture has a central controller that manages RUs for all MBSs and UABSs in the considered area. Therefore, the controller has the ability to predict the interference coming from all links GUE-MBS and GUE-UABS. In the following, to tackle these issues and implement a proper RRM, we propose four ILP problems related to the

distributed or centralized architectures as well as the potential reuse of RUs from which we achieve the optimal solution and maximize network performance.

IV. Problem Statement

In the following, we present four ILP formulations, denoted respectively as $\mathcal{P}1$, $\mathcal{P}2$, $\mathcal{P}3$, and $\mathcal{P}4$, which correspond to two architectures and two resource utilization approaches, as described in the previous section. Despite their slight differences, all four ILPs aim for the same target performance and share a similar network model. We describe their structure by introducing a common objective function and desired outputs. The optimal RRM strategy is obtained by solving these formulations at regular intervals of duration Δt. The objective is to maximize the number of *served* GUEs within Δt through a joint operation of MBS and UABS, taking into account the cost factor associated with activating each UABS. Given the discussion on RUs and interference, we still have some degrees of freedom related to i) the BS from which a GUE has assigned RUs, ii) how many RUs should be allocated given the demand D_g, iii) the UABSs' beams that should be activated, iv) and the number of RUs needed by backhaul links given its capacity or data rate. These aspects are then considered in the proposed ILP, which results in a beam selection and joint resource allocation optimization accounting for the backhaul capacity.

We now describe the variables used to introduce the ILP. First, the binary variables are defined as follows:

$$x_{g,m} = \begin{cases} 1 & \text{if user } g \in \mathcal{G} \text{ is assigned RUs by} \\ & \text{MBS } m \in \mathcal{M} \\ 0 & \text{otherwise} \end{cases}$$

$$x_{g,a} = \begin{cases} 1 & \text{if user } g \in \mathcal{G} \text{ is assigned RUs by} \\ & \text{UABS } a \in \mathcal{A} \\ 0 & \text{otherwise} \end{cases}$$

$$x_{a,m} = \begin{cases} 1 & \text{if UABS } a \in \mathcal{A} \text{ is assigned RUs by} \\ & \text{MBS } m \in \mathcal{M} \\ 0 & \text{otherwise} \end{cases}$$

$$e_{j_a} = \begin{cases} 1 & \text{if beam } j_a \in \mathcal{K} \text{ is active on} \\ & \text{UABS } a \in \mathcal{A} \\ 0 & \text{otherwise} \end{cases}$$

$$\iota_{g,m,a'} = \begin{cases} 1 & \text{if link } g - m \text{ is interfered by any} \\ & \text{GUE connected to } a' \in \mathcal{A} \\ 0 & \text{otherwise} \end{cases}$$

$$\iota_{g,a,m'} = \begin{cases} 1 & \text{if link } g - a \text{ is interfered by any} \\ & \text{GUE connected to } m' \in \mathcal{M} \\ 0 & \text{otherwise} \end{cases}$$

$$\iota_{g,m,m'} = \begin{cases} 1 & \text{if link } g - m \text{ is interfered by any} \\ & \text{GUE connected to } m' \in \mathcal{M} \\ 0 & \text{otherwise} \end{cases}$$

$$\iota^{(b)}_{m,a} = \begin{cases} 1 & \text{if MBS } m \in \mathcal{M} \text{ suffers interference} \\ & \text{from any GUE connected to } a \in \mathcal{A} \\ 0 & \text{otherwise} \end{cases}$$

$$\iota^{(b)}_{a,m} = \begin{cases} 1 & \text{if UABS } a \in \mathcal{A} \text{ suffers interference} \\ & \text{from any GUE connected to } m \in \mathcal{M} \\ 0 & \text{otherwise} \end{cases}$$

$$\iota^{(b)}_{m,m'} = \begin{cases} 1 & \text{if MBS } m \in \mathcal{M} \text{ suffers interference} \\ & \text{from any GUE connected to } m' \in \mathcal{M} \\ 0 & \text{otherwise} \end{cases}$$

The following integer variables, along with binary variables, are optimized and serve as the output of the RRM procedure, providing the RUs allocation for each communication link:

- $w_{g,m}$ and $w_{g,a}$ represent the number of RUs assigned to user $g \in \mathcal{G}$ by $m \in \mathcal{M}$ or $a \in \mathcal{A}$, respectively;
- $w_{a,m}$ is the number of resources assigned by the MBS $m \in \mathcal{M}$ to the backhaul with UABS $a \in \mathcal{A}$.

As previously stated, the objective function aims at maximizing the number of served users, through y_g, defined as:

$$y_g = \begin{cases} 1 & \text{if user } g \in \mathcal{G} \text{ is served} \\ 0 & \text{otherwise} \end{cases}$$

To achieve continuous service for vehicles, we assign a time-varying priority value, denoted as p_g, to each user $g \in \mathcal{G}$. Specifically, for each $t \in [1, T_w]$, p_g varies as follows:

$$p_g(t) = \begin{cases} 1 & \text{for } t = 1 \\ p_g(t-1) + 1 & \text{if } y_g(t) = 1 \\ p_g(t-1) & \text{if } y_g(t) = 0 \end{cases}$$

To consider the impact of the activation of UABSs, we introduce the parameter ξ as a weighting factor ranging between [0;1]. Such a factor allows us to assess the influence of having multiple UABSs active in the network. Additionally, we incorporate two normalization factors, namely N_{ue} and N_{uav}, representing the number of GUEs and UAVs respectively. Furthermore, a dynamic normalizing factor $p^{(\Delta t)}_{g,max}$ is introduced to balance the priority term in the objective function. This factor linearly increases between [1;N_{s}] as the GUE p_g increases over each window $N_{\text{s}}\Delta t$. In general, it is possible to eliminate the impact of the cost factor on UABS activation by setting $N_{\text{ue}} = 1$ and $\xi = 0$. In summary, the ILPs aim to optimize: i) the joint operation between MBSs and UABSs by maximizing y_g with variables $x_{g,m}$, $w_{g,m}$, $x_{g,a}$, $w_{g,a}$; ii) the selection of UABSs' beams to maximize the number of GUEs using variables e_{j_a}; iii) the assignment of RB to backhaul with variables $w_{a,m}$, considering all $g \in \mathcal{G}$, $a \in \mathcal{A}$, $m \in \mathcal{M}$ and iv) the activation of UABSs based on the value of ξ, determining which UAV serves as UABS.

For what concerns the model complexity, the problem is NP-hard even in the special case with a single UABS and a single MBS, and all GUEs visible by the UABS and the MBS. In fact, the problem generalizes the Multiple Knapsack Problem that is known to be strongly NP-hard also for the special case of two knapsacks [36], [37].

A. Case I: Distributed with Resource Split

The RRM algorithm runs separately at each MBS $m \in \mathcal{M}$, so it is dependent on m. Each MBS manages the RUs of a given set $\mathcal{G}_m$ of GUEs, and a given set $\mathcal{A}_m$ of UABSs. These sets are determined by the GUEs and UABSs, which select the MBS granting them the strongest communication

link, i.e., highest SNR. This is later described in Fig. 5. The environment information exchanged by MBSs is limited to the total number of UAVs present in the area since this information is necessary to avoid interference between the different UAVs. We formulate the problem $\mathcal{P}1$ as:

$$\mathcal{P}1: \max \left(\sum_{g \in \mathcal{G}_m} \frac{1-\xi}{N_{\text{ue}}} y_g p_g - \sum_{a \in \mathcal{A}_m} \frac{\xi}{N_{\text{uav}}} x_{a,m} p_{g,max}^{(\Delta t)} \right) \tag{7a}$$

s.t.: $w_{g,m} r_{g,m} \Delta t +$

$$+ \sum_{a \in \mathcal{A}} \sum_{j_a \in \mathcal{K}_a} k_{g,j_a} w_{g,a} r_{g,a} \Delta t \geq y_g D_g, \, \forall g \in \mathcal{G}_m \tag{7b}$$

$$\sum_{g \in \mathcal{G}_m} w_{g,m} + \sum_{a \in \mathcal{A}_m} w_{a,m} \leq W_m^* \tag{7c}$$

$$\sum_{g \in \mathcal{G}_m} k_{g,j_a} w_{g,a} + w_{a,m} \leq W_a^*, \quad \forall a \in \mathcal{A}_m, \, \forall j_a \in \mathcal{K}_a \tag{7d}$$

$$\sum_{g \in \mathcal{G}_m} \sum_{j_a \in \mathcal{K}_a} w_{g,a} k_{g,j_a} r_{g,a} \leq r_{a,m} w_{a,m}, \quad \forall a \in \mathcal{A}_m \tag{7e}$$

$$\sum_{j \in \mathcal{K}_a} e_{j_a} \leq N_{\text{beam}}, \quad \forall a \in \mathcal{A}_m \tag{7f}$$

$$\sum_{g \in \mathcal{G}_m} w_{g,a} k_{g,j_a} \leq e_{j_a} W_a^*, \quad \forall a \in \mathcal{A}_m, \, \forall j_a \in \mathcal{K}_a \tag{7g}$$

$$x_{g,m} + \sum_{a \in \mathcal{A}} x_{g,a} \leq 1, \quad \forall g \in \mathcal{G}_m \tag{7h}$$

$$w_{g,m} \leq x_{g,m} W_m^*, \quad \forall g \in \mathcal{G}_m \tag{7i}$$

$$w_{g,a} \leq x_{g,a} W_a^*, \quad \forall a \in \mathcal{A}_m, \, \forall g \in \mathcal{G}_m \tag{7j}$$

$$x_{g,a} \in \{0,1\}, \quad \forall a \in \mathcal{A}_m, \, \forall g \in \mathcal{G}_m \tag{7k}$$

$$x_{g,m} \in \{0,1\}, \quad \forall g \in \mathcal{G}_m \tag{7l}$$

$$x_{a,m} \in \{0,1\}, \quad \forall a \in \mathcal{A}_m \tag{7m}$$

$$w_{g,a} \in \{0, W_a^*\}, \quad \forall a \in \mathcal{A}_m, \, \forall g \in \mathcal{G}_m \tag{7n}$$

$$w_{g,m} \in \{0, W_m^*\}, \quad \forall g \in \mathcal{G}_m \tag{7o}$$

$$w_{a,m} \in \{0, \min[W_m^*, W_a^*]\}, \quad \forall a \in \mathcal{A}_m \tag{7p}$$

where the input k_{g,j_a} indicates with value 1 whether vehicle g is covered by beam j_a of UABS $a \in \mathcal{A}_m$ and 0 otherwise. Sets $\mathcal{A}_m \subseteq \mathcal{A}$ and $\mathcal{G}_m \subseteq \mathcal{G}$ depend on m and are computed later in Sec.V. Each constraint serves a specific purpose. Constraint (7b) ensures that each vehicle g transmits a demand of D_g bits, considering the rate of a unitary RU and the number of assigned RUs from a particular BS. Constraints (7c) and (7d) limit the number of RUs assigned to respect the maximum capacity of MBSs and UABSs, respectively, accounting for backhaul RUs as well. Constraint (7e) ensures sufficient backhaul capacity for UABS vehicular traffic. Constraints (7f) and (7g) restrict the number of activated beams at each UABS $a \in \mathcal{A}_m$ to N_{beam}. Finally, constraints (7h) to (7j) ensure that each vehicle is served by only one BS at a time. Expressions (7k)-(7p) demonstrate the validity of each variable in $\mathcal{P}1$.

B. Case II: Distributed with Resource Sharing

As the RRM algorithm of the distributed architecture runs at the single MBS, the objective function of $\mathcal{P}2$ is the same. Due to the lack of awareness of interference sources from other MBSs, there are no specific inputs to the relative ILP. Still, when RUs are shared from a common pool for the GUE-UABSs and GUE-MBS links, the interference coming from the links managed by the same MBS is known. Therefore, $\mathcal{P}2$ is mathematically described as follows.

$$\mathcal{P}2: \max \left(\sum_{g \in \mathcal{G}_m} \frac{1-\xi}{N_{\text{ue}}} y_g p_g - \sum_{a \in \mathcal{A}_m} \frac{\xi}{N_{\text{uav}}} x_{a,m} p_{g,max}^{(\Delta t)} \right) \tag{8a}$$

s.t.: $w_{g,m} r_{g,m,a'}^{\text{I}} \Delta t + \sum_{a \in \mathcal{A}_m} \sum_{j_a \in \mathcal{K}_a} k_{g,j_a} w_{g,a} r_{g,a,m}^{\text{I}} \Delta t \geq$

$$\geq \left(\iota_{g,m,a'} + \sum_{a \in \mathcal{A}_m} \iota_{g,a,m} \right) D_g, \, \forall g \in \mathcal{G}_m, \forall a' \in \mathcal{A}_m \tag{8b}$$

(7b) - (7g)

$$\iota_{m,a}^{(\text{b})} \geq \sum_{g' \in \mathcal{G}_m} \frac{I_{g',a,m} x_{g',a}}{I_{g',a,m}}, \, \forall a \in \mathcal{A}_m \tag{8c}$$

$$\iota_{a,m}^{(\text{b})} \geq \sum_{g' \in \mathcal{G}_m} \frac{I_{g',m,a} x_{g',m}}{I_{g',m,a}}, \, \forall a \in \mathcal{A}_m \tag{8d}$$

$$\iota_{g,m,a} \geq x_{g,m} + \iota_{m,a}^{(\text{b})} - 1, \, \forall g \in \mathcal{G}_m, \forall a \in \mathcal{A}_m \tag{8e}$$

$$\iota_{g,a,m} \geq x_{g,a} + \iota_{a,m}^{(\text{b})} - 1, \, \forall g \in \mathcal{G}_m, , \, \forall a \in \mathcal{A}_m \tag{8f}$$

$$\iota_{m,a}^{(\text{b})}, \iota_{a,m}^{(\text{b})} \in \{0,1\}, \, \forall a \in \mathcal{A}_m \tag{8g}$$

$$\iota_{g,m,a}, \iota_{g,a,m} \in \{0,1\}, \, \forall g \in \mathcal{G}_m, \forall a \in \mathcal{A}_m \tag{8h}$$

(7h) - (7p)

With respect to $\mathcal{P}1$, $\mathcal{P}2$ includes resource sharing and, thus, the possible interference prediction at the single MBS. Therefore, new variables must be introduced, like $\iota_{a,m}^{(\text{b})}$, $\iota_{m,a}^{(\text{b})}$, $\iota_{g,a,m}$, and $\iota_{g,m,a'}$. Additionally, $r_{g,m,a'}^{\text{I}}$ denotes the data rate achieved by the link g-m when it is interfered by the strongest possible interferer connected to a', as formulated in Eq. (2); $I_{g',a,m}$ and $I_{g',m,a}$ have binary values stating if $a \in \mathcal{A}$ is inside the interfering beam of $g' \in \mathcal{G}$ while connected to m or m is inside the interfering beam of $g' \in \mathcal{G}$ while connected to $a \in \mathcal{A}$, respectively (1 if true, 0 otherwise). The constraint (8b) is similar to (7b) as it defines the number of resources required by GUE g to satisfy its demand, D_g; however, (8b) serves to recompute the number of RUs required only in the case interference is present, i.e., g is connected to an interfered BS. Description of constraints (7b) - (7g) are reported in Sec.IV-A. Ensuring the efficient transmission of data in our vehicular communication model involves several constraints. Firstly, constraint (7b) guarantees that each vehicle g transmits a demand of D_g bits. This considers the rate of a unitary RU and the number of assigned RUs from a specific BS. To maintain network integrity, constraints (7c) and (7d) place limits on the number of RUs assigned, respecting the maximum capacity of both MBSs and UABSs, while accounting for backhaul RUs.

Moreover, constraint (7e) ensures that there is adequate backhaul capacity to support vehicular traffic at UABS. Lastly, constraints (7f) and (7g) serve to restrict the number of activated beams at each UABS denoted by $a \in \mathcal{A}_m$ to a fixed value of N_{beam}. Then, the constraints (8c) and (8d) verify if there is at least one effective interferer on the MBS that is

connected to a UABSs $a \in \mathcal{A}_m$ or vice versa, respectively, and constraints 8e and (8f) verify if a UABS $a \in \mathcal{A}_m$ is interfering the link $g-m$ given it is established or if the MBS m is interfering the link $g-a,\ a \in \mathcal{A}_m$ given it is established, respectively. Finally, constraints (8g) - (8h) and (7h) - (7p), the same constraints used in $\mathcal{P}1$, specify all binary variables.

C. Case III: Centralized with Resource Split

The centralized RRM algorithm, operating at the network core, possesses knowledge of all the BSs. This allows a better MBSs load balance, understanding the potential interference that each network element may generate. The problem formulated for the centralized architecture is denoted as $\mathcal{P}3$.

$$\mathcal{P}3 : \max \left(\sum_{g \in \mathcal{G}} \frac{1-\xi}{N_{\text{ue}}} y_g p_g - \sum_{a \in \mathcal{A}} \sum_{m \in \mathcal{M}} \frac{\xi}{N_{\text{uav}}} x_{a,m} p_{g,max}^{(\Delta t)} \right) \tag{9a}$$

$$\textbf{s.t.:} \sum_{m \in \mathcal{M}} w_{g,m} r_{g,m} \Delta t + \sum_{a \in \mathcal{A}} \sum_{j_a \in \mathcal{K}_a} k_{g,j_a} w_{g,a} r_{g,a} \Delta t \geq + \geq y_g D_g,\ \forall g \in \mathcal{G} \tag{9b}$$

$$\sum_{m \in \mathcal{M}} w_{g,m} r^{\text{I}}_{g,m,m'} \Delta t \geq \left(\sum_{m \in \mathcal{M}} \iota_{g,m,m'} \right) D_g, \quad \forall g \in \mathcal{G}, \forall m' \in \mathcal{M} \tag{9c}$$

$$\sum_{g \in \mathcal{G}} w_{g,m} + \sum_{a \in \mathcal{A}} w_{a,m} \leq W^*_m,\ \forall m \in \mathcal{M} \tag{9d}$$

$$\sum_{g \in \mathcal{G}} k_{g,j_a} w_{g,a} + \sum_{m \in \mathcal{M}} w_{a,m} \leq W^*_a,\ \forall a \in \mathcal{A},\ \forall j_a \in \mathcal{K}_a \tag{9e}$$

$$\sum_{g \in \mathcal{G}} \sum_{j_a \in \mathcal{K}_a} w_{g,a} k_{g,j_a} r_{g,a} \leq \sum_{m \in \mathcal{M}} r_{a,m} w_{a,m},\ \forall a \in \mathcal{A} \tag{9f}$$

$$\sum_{j \in \mathcal{K}_a} e_{j_a} \leq N_{\text{beam}},\ \forall a \in \mathcal{A} \tag{9g}$$

$$\sum_{g \in \mathcal{G}} w_{g,a} k_{g,j_a} \leq e_{j_a} W^*_a,\ \forall a \in \mathcal{A},\ \forall j_a \in \mathcal{K}_a \tag{9h}$$

$$\iota^{(\text{b})}_{m,m'} \geq \sum_{g' \in \mathcal{G}} \frac{I_{g',m',m} x_{g',m'}}{I_{g',m',m}},\ \forall m, m' \in \mathcal{M} \tag{9i}$$

$$\iota_{g,m,m'} \geq x_{g,m} + \iota^{(\text{b})}_{m,m'} - 1, \forall g \in \mathcal{G}, \forall m, m' \neq m \in \mathcal{M} \tag{9j}$$

$$\sum_{m \in \mathcal{M}} x_{g,m} + \sum_{a \in \mathcal{A}} x_{g,a} \leq 1,\ \forall g \in \mathcal{G} \tag{9k}$$

$$w_{g,m} \leq x_{g,m} W^*_m, \forall m \in \mathcal{M}, \forall g \in \mathcal{G} \tag{9l}$$

$$w_{g,a} \leq x_{g,a} W^*_a, \forall a \in \mathcal{A}, \forall g \in \mathcal{G} \tag{9m}$$

$$\sum_{m \in \mathcal{M}} x_{a,m} \leq 1, \forall a \in \mathcal{A} \tag{9n}$$

$$w_{a,m} \leq x_{a,m} W^*_m, \forall m \in \mathcal{M}, \forall a \in \mathcal{A} \tag{9o}$$

$$x_{g,a} \in \{0,1\}, \forall a \in \mathcal{A}, \forall g \in \mathcal{G} \tag{9p}$$

$$x_{g,m} \in \{0,1\}, \forall m \in \mathcal{M}, \forall g \in \mathcal{G} \tag{9q}$$

$$x_{a,m} \in \{0,1\}, \forall m \in \mathcal{M}, \forall a \in \mathcal{A} \tag{9r}$$

$$w_{g,a} \in \{0, W^*_a\}, \forall a \in \mathcal{A}, \forall g \in \mathcal{G} \tag{9s}$$

$$w_{g,m} \in \{0, W^*_m\}, \forall m \in \mathcal{M}, \forall g \in \mathcal{G} \tag{9t}$$

$$w_{a,m} \in \{0, \min[W^*_m, W^*_a]\}, \forall m \in \mathcal{M}, \forall a \in \mathcal{A} \tag{9u}$$

The constraints Eqs. (9b)-(9m) find their correspondent in Eqs. (7b)-(7j). Thus, the description and motivation of these constraints are the same, with the difference that the optimization includes the overall set of MBSs, $\mathcal{M}$, together with the knowledge of their surrounding environment. Indeed, the algorithm is centralized and it can optimize the control over the entire network scenario. Also, since MBSs use RU reuse equal to 1, the controller is able to predict the interference that potentially arises among the different MBSs. This is taken into account in i) constraint (9c) for what concerns the number of RUs, as similar to (8b), ii) constraint (9i) for looking if there is at least one interferer on an other MBS, and iii) constraint (9j) for defining if there is interference on an established link. Furthermore, two more constraints are added: Eqs. (9n) and (9o). These two ensure that the backhaul for each active UABS is established with a single MBS. Clearly, the ILP formulated for the centralized case adds more levels of complexity depending on the new variables and constraints introduced by the set $\mathcal{M}$. The model does not vary for higher values of the cardinality, $|\mathcal{M}|$, but the computation time might increase exponentially, limiting its practical implementation over large network areas.

D. Case IV: Centralized with Resource Sharing

The problem formulated for the centralized architecture implementing resource sharing is denoted as $\mathcal{P}4$.

$$\mathcal{P}4 : \max \left(\sum_{g \in \mathcal{G}} \frac{1-\xi}{N_{\text{ue}}} y_g p_g - \sum_{a \in \mathcal{A}} \sum_{m \in \mathcal{M}} \frac{\xi}{N_{\text{uav}}} x_{a,m} p_{g,max}^{(\Delta t)} \right) \tag{10a}$$

$$\textbf{s.t.:} \sum_{m \in \mathcal{M}} w_{g,m} r^{\text{I}}_{g,m,a'} \Delta t + \sum_{a \in \mathcal{A}} \sum_{j_a \in \mathcal{K}_a} k_{g,j_a} w_{g,a} r^{\text{I}}_{g,a,m'} \Delta t \geq \left(\sum_{m \in \mathcal{M}} \iota_{g,m,a'} + \sum_{a \in \mathcal{A}} \iota_{g,a,m'} \right) D_g, \quad \forall g \in \mathcal{G}, \forall a' \in \mathcal{A}, \forall m' \in \mathcal{M} \tag{10b}$$

(9b) - (9h)

$$\iota^{(\text{b})}_{m,a} \geq \sum_{g' \in \mathcal{G}} \frac{I_{g',a,m} x_{g',a}}{I_{g',a,m}},\ \forall a \in \mathcal{A},\ \forall m \in \mathcal{M} \tag{10c}$$

$$\iota^{(\text{b})}_{a,m} \geq \sum_{g' \in \mathcal{G}} \frac{I_{g',m,a} x_{g',m}}{I_{g',m,a}},\ \forall a \in \mathcal{A}, \forall m \in \mathcal{M} \tag{10d}$$

$$\iota_{g,m,a} \geq x_{g,m} + \iota^{(\text{b})}_{m,a} - 1,\ \forall g \in \mathcal{G},\ \forall a \in \mathcal{A}, \forall m \in \mathcal{M} \tag{10e}$$

$$\iota_{g,a,m} \geq x_{g,a} + \iota^{(\text{b})}_{a,m} - 1,\ \forall g \in \mathcal{G},\ \forall a \in \mathcal{A}, \forall m \in \mathcal{M} \tag{10f}$$

$$\iota^{(\text{b})}_{m,a}, \iota^{(\text{b})}_{a,m} \in \{0,1\} \quad \forall a \in \mathcal{A},\ \forall m \in \mathcal{M} \tag{10g}$$

$$\iota_{g,m,a}, \iota_{g,a,m} \in \{0,1\},\ \forall g \in \mathcal{G}, \forall a \in \mathcal{A}, \forall m \in \mathcal{M} \tag{10h}$$

(9k) - (9u)

The constraint (10b) is similar to (8b) as reuse of RUs is present. Description of constraints (9b) - (9h) are reported in Sec.IV-C. These constraints collectively ensure the efficient transmission of data and the optimal utilization of resources. They address considerations such as individual vehicle demands, the assignment and limitation of resource units (RUs) from specific BSs, and the overall capacity constraints of both MBSs and UABSs. Additionally, the constraints account for

the sufficient backhaul capacity required for UABS vehicular traffic. The control over the number of activated beams at each UABS is also constrained to a specified limit, contributing to the overall system's stability and performance. Then, the constraints (10c) and (10d) verify if there is at least one effective interferer on the MBS that is connected to a UABSs $a \in \mathcal{A}$ or vice versa, respectively, and constraints 10e and (10f) verify if a UABS $a \in \mathcal{A}$ is interfering the link $g - m$ given it is established, or if the MBS m is interfering the link $g - a,\ a \in \mathcal{A}$ given it is established, respectively. The difference with respect to the constraints (8c) to (8f) is that the entire set of UABSs and GUEs is under control. Finally, the constraints (10g) - (10h) and (9k) - (9u), the same constraints used in $\mathcal{P}3$, specify all binary variables.

V. Problem Implementation

Due to the complexity of the scenario considered, some assumptions have been introduced in order to simplify the solution of the ILP. In particular, since considering all potential interference exponentially increases the ILP complexity, we feed it with the strongest interferer for each potential useful link. The strongest interferer is selected based on time frequency and space dimension, considering beam directivity. This simplifying assumption allows decreasing the number of input parameters and the set of variables of the ILP. To derive the actual performance of the network, we apply the methodology depicted in Fig. 5: i) we first run the ILP, having as input time parameters $N_{\mathrm{w}}, T_{\mathrm{sim}}$, all unitary rates $r_{x,y}$, user demand D_g, beam directivity k_{g,j_a} and resource availability W_x^*; ii) the output of the ILP, including the set of RUs used by every BSs to serve the vehicles or to support backhauling, $w_{x,y}$ and the number of UABSs to be activated $x_{a,m}$, are given as input to a network simulator, where all assumptions are dropped to compute $P_g^{(sat)}$. Moreover, as explained below, the updated value of the GUEs priorities goes in input to the ILP in the following Δt.

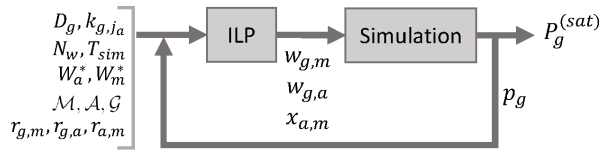

Fig. 5. Simulation block scheme.

Algorithm 1 clarifies the relationship between the ILP and the simulation, specifying the latter's features. In particular, the ILP gives information on the number of resources used to serve each GUE in each Δt, but does not provide information on which RUs are actually used in *Time x Frequency x Space* (t,f,s). As explained in Algorithm 1, at each Δt, once we know how many RUs are used by each BS to serve every GUEs, we create two matrices, $\mathcal{W}_a$ and $\mathcal{W}_m$, respectively for UABSs and MBSs (lines 6-12), used to assess the actual RUs. We do not account for resources used for backhaul $w_{a,m}$, assuming orthogonality. Once all resources are assigned, we compute the intra-link interference, based on time, frequency and space, and check whether $\gamma_g^{(I)}$ is below the defined threshold (lines 14-17). Finally, each vehicle served will have an increased value of priority in the following Δt (lines 18-22).

Algorithm 1: ILP and Simulation.

1 **Input:** $\mathcal{M}$, $\mathcal{A}$, $\mathcal{G}$, k_{g,j_a}, D_g, W_a^*, W_m^*, $N_{\mathrm{w}}, T_{\mathrm{sim}}$, $r_{g,m},\ r_{a,m},\ r_{g,a}\ \forall g \in \mathcal{G},\ a \in \mathcal{A},\ m \in \mathcal{M}$
2 **Output:** $P_g^{(sat)}\ \forall g \in \mathcal{G}$
3 **for** $t = t_0$ *to* T_{sim} **do**
4 *run* ***ILP***
5 *start* ***Simulator***
6 **for** *each MBS* $m \in \mathcal{M}$ **do**
7 create array $\mathcal{W}_m$ of length $W_m^* - \sum_{a \in \mathcal{A}} w_{a,m}$
8 map $w_{g,m}$ in $\mathcal{W}_m$, $\forall g \in \mathcal{G}$
9 **end**
10 **for** *each UABS* $a \in \mathcal{A}$ **do**
11 create array $\mathcal{W}_a$ of length $W_a^* - \sum_{m \in \mathcal{M}} w_{a,m}$
12 map $w_{g,a}$ in $\mathcal{W}_a$, $\forall g \in \mathcal{G}$
13 **end**
14 **for** *each GUE* $g \in \mathcal{G}$ **do**
15 compute $\gamma_g^{(I)}$
16 set $y_g = 1$ if $\gamma_g^{(I)} \geq \gamma_{th}^{(I)}$
17 **end**
18 **for** *each GUE* $g \in \mathcal{G}$ **do**
19 **if** $(t\ mod\ N_{\mathrm{w}}) = 0$ **then**
20 $p_g = 1$
21 **else if** $y_g = 1$ *and* $1 \leq (t\ mod\ N_{\mathrm{w}}) < N_{\mathrm{w}}$ **then**
22 $p_g += 1$
23 **end**
24 *stop* ***Simulator***
25 **end**

VI. Numerical Results

Numerical results will be discussed in the following, showing the general improvement obtained in the performance when deploying UABSs in the network and analyzing the configurations discussed above. Simulations of the proposed model and scenario run in a Python environment, and the Gurobi solver provides the output from the ILP. Each simulation spans over a time $T_{\mathrm{sim}} = 60$ seconds and parameter settings are listed in Table III. To properly account for vehicular movement through time, we implement vehicular traces obtained from SUMO, "Simulation of Urban MObility", which is an open-source, highly portable, microscopic, and continuous traffic simulation package designed to handle large networks [38], which is a common approach exploited to solve similar problems [39], [40].

In the following, we show the percentage of satisfied users, $P_g^{(sat)}$, that is the ratio between the number of GUEs for which it holds $N_{\mathrm{s}} \geq \hat{N}_{\mathrm{s}}$, w.r.t. the total number of GUEs in the area.

In this section, we will present all results related to the distributed and the centralized model, in which interference is taken into account.

Figs. 6, 7, 8 show the percentage of satisfied GUEs, $P_g^{(sat)}$, depending on the minimum number of intervals of duration Δt given by the application requirements, $\hat{N}_{\mathrm{s}}$, chosen over the time window T_{w}. All curves present a decreasing trend when increasing $\hat{N}_{\mathrm{s}}$, and, in particular, Fig. 6 shows how sharing resources is more efficient than splitting the pool of RUs, even with higher interference. Due to the nature of the distributed

TABLE III
NETWORK AND CHANNEL PARAMETERS.

Parameter	Notation	Value
Area sides	QxQ'	1800x1600 m
Number of MBSs	$\lvert\mathcal{M}\rvert$	4
Number of UAVs	$\lvert\mathcal{A}\rvert = N_{\text{uav}}$	18
SNR threshold	γ_{th}	-13.7 dB
SINR threshold	γ^I_{th}	-5 dB
UABS transmit power	$P_{\text{tx,A}}$	23 dBm
GUE transmit power	$P_{\text{tx,G}}$	20 dBm
UABS transmission gain	$G_{\text{tx,A}}$	17.72 dB
UABS receiver gain	$G_{\text{rx,A}}$	17.72 dB
GUE transmission gain	$G_{\text{tx,G}}$	0 dB
Paparazzi-scan sensing radius	r_{p}	200 m
Paparazzi-scan time shift	t_{p}	25 s
Inter-UAV distance	d_{UAV}	500 m
UABS speed	v_A	20 m/s
UABS altitude	h	100 m
UABS aperture angle	α_{A}	140°
Nr. of UABS available beams	K	9
Max n. of UABS active beams	N_{beam}	4
GUE traffic demand	D_g	100 kbit
Effective noise power	P_{noise}	-106.4 dBm
Overall bandwidth	B	400 MHz
Channel bandwidth	B_{ch}	1.44 MHz
Subcarrier spacing	Δf	120 kHz
Slot duration	T_{slot}	0.125 ms
Nr. of time windows for QoE	N_{w}	60

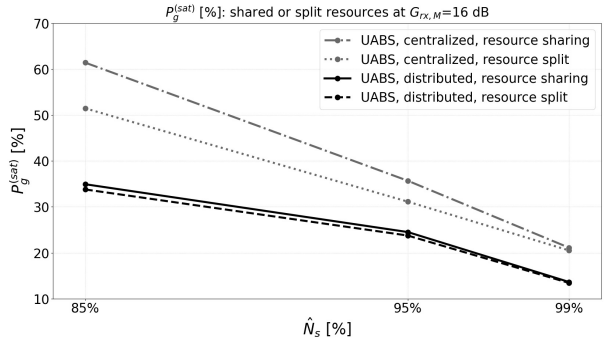

Fig. 6. Percentage of satisfied GUEs, $P_g^{(sat)}$, while varying the QoE threshold, $\hat{N}_{\text{s}}$, and for different parameter settings and $G_{\text{rx,M}} = 16$ dB, with the inclusion of interference.

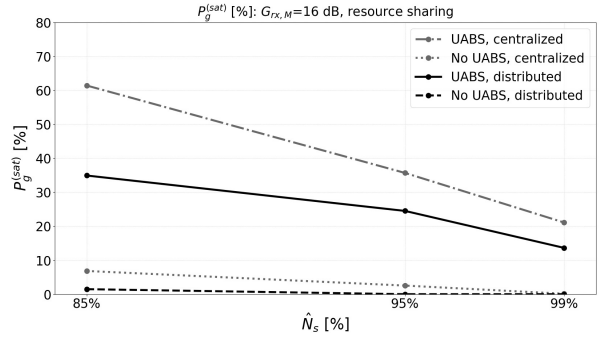

Fig. 7. Percentage of satisfied GUEs, $P_g^{(sat)}$, while varying the QoE threshold, $\hat{N}_{\text{s}}$, and for different parameter settings and $G_{\text{rx,M}} = 16$ dB, with the inclusion of interference.

model, MBSs share worst-case, non-real-time information on interference toward other MBSs, the improvement between resource split and sharing is lower than in the centralized case,

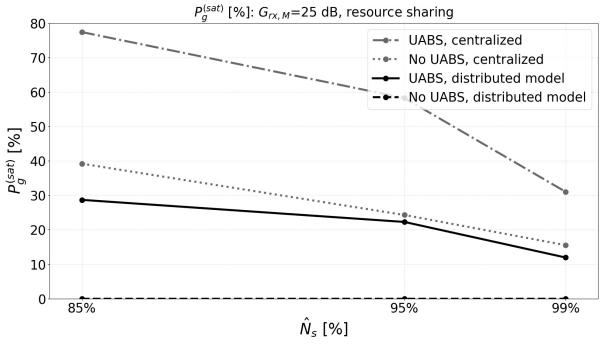

Fig. 8. Percentage of satisfied GUEs, $P_g^{(sat)}$, while varying the QoE threshold, $\hat{N}_{\text{s}}$, and for different parameter settings and $G_{\text{rx,M}} = 25$ dB, with the inclusion of interference.

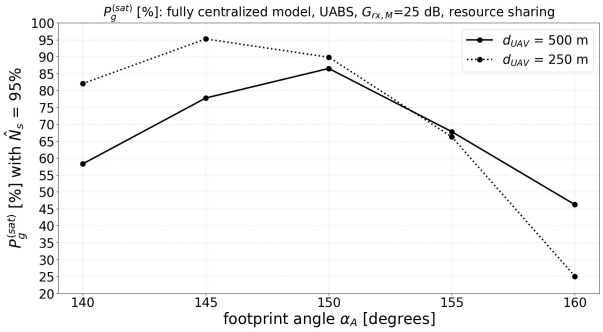

Fig. 9. Percentage of satisfied GUEs, $P_g^{(sat)}$, for the same QoE threshold, $\hat{N}_{\text{s}} = 95\%$, and for different UABS aperture angles.

where proper load balancing is performed.

Since resource sharing globally performs better than resource split results, Figs. 7 and 8 only show results related to the former. The difference between the two graphs is the value of the receiving MBS gain $G_{\text{rx,M}}$ which is equal to 16 dB and 25 dB, respectively.

We can notice how the use of the centralized architecture collectively improves the results with both values of $G_{\text{rx,M}}$. For instance, in Fig. 7, having a controller which has a whole overview of the scenario allows us to increase GUEs satisfaction levels of 20% when $\hat{N}_{\text{s}}$ is set to 85%, proving the goodness of the centralized configuration. Moreover, the comparison with the benchmark case, in which GUEs are served only by MBSs, shows that the use of UABSs in the scenario significantly improves network performance. In particular, in Fig. 8, $P_g^{(sat)}$ increases up to 80% when UAVs start working as UABSs. Finally, increasing $G_{\text{rx,M}}$ from 16 to 25 dB causes opposite effects for the two architectures: as mentioned above, due to the nature of the distributed model, higher receiving gain at the MBS means higher non-real-time interference, while in the centralized case, the ILP is able to tackle the current interference.

Fig. 9 shows the percentage of satisfied GUEs, $P_g^{(sat)}$ for a fixed value of $\hat{N}_{\text{s}}$, depending on different UABSs aperture angles (which corresponds to varying the UABSs flight height). The two curves are obtained for two values of inter-UAV distance: d_{UAV} equal to 500 m, and d_{UAV} equal to 250 m. Reducing the inter-UAV distance causes the maximum value

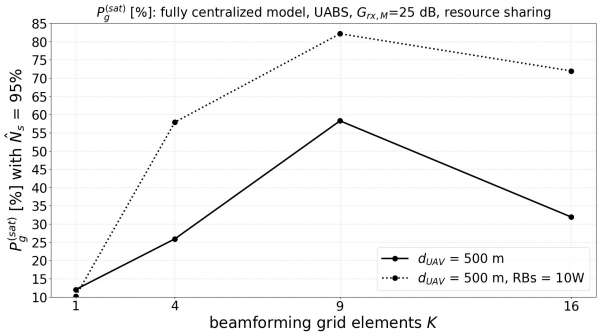

Fig. 10. Percentage of satisfied GUEs, $P_g^{(sat)}$, for the same QoE threshold, $\hat{N}_\mathrm{s} = 95\%$, and for different beam grids.

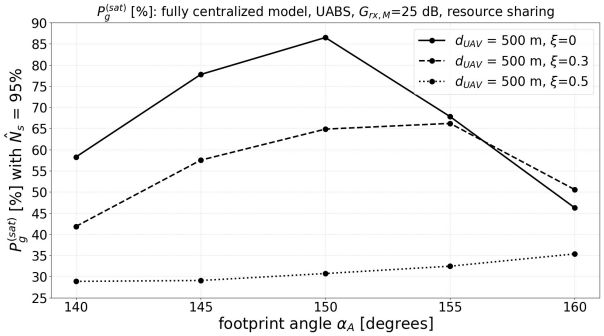

Fig. 11. Percentage of satisfied GUEs, $P_g^{(sat)}$, for the same QoE threshold, $\hat{N}_\mathrm{s} = 95\%$, and for different UABS aperture angles, including cost.

of $P_g^{(sat)}$ to be higher and shifted to the left. This implies that, despite the increased overlapping, the ILP is able to manage a higher level of interference, as long as the footprint is below 155 degrees, where the performance drop due to an increased overlap with respect to when d_{UAV} is equal to 500 m.

Figure 10 demonstrates the influence of beamforming configuration on network performance by examining various grid of beams and network capacities. It is evident that the impact of beamforming is heavily reliant on the availability of backhaul resources. Specifically, a larger number of RBs enables the BS to effectively handle more demanding signalling processing, highlighting the critical role played by backhaul resources. Results display how, for a fixed value of $\hat{N}_\mathrm{s}$, $P_g^{(sat)}$ varies by changing the number of beams in the antenna array on the UABS. Due to the relationship between the antenna gain and the number of beams, as explained in Eq. (6), having a higher number of beams performs better with respect to a single antenna scenario, but at the same time too many beams, make the backhaul signalling too heavy. Moreover, by increasing the availability of RUs by a factor of 10, the gap between $P_g^{(sat)}$ between 9 and 16 beam grid reduces from 30% to 10%.

Fig. 11 shows the percentage of satisfied GUEs, $P_g^{(sat)}$ for a fixed value of $\hat{N}_\mathrm{s}$, depending on different UABSs aperture angles. The three curves are obtained for three values of ξ: 0, 0.3 and 0.5. Increasing the value of ξ means that the cost of UABSs activation will be higher, and the general trend of $P_g^{(sat)}$ reduces. It is important to notice that for higher aperture angles, implementing a higher cost might be useful, since interference is handled more effectively. Increasing ξ causes the maximum value of $P_g^{(sat)}$ to be lower and shifted to the right. This implies that, despite the increased overlapping, the ILP is able to manage a higher level of interference, as long as the best set of UABSs is turned on.

VII. Conclusion

In this work we propose a novel approach to minimize uplink interference in vehicular networks, when considering a complex urban scenario, where terrestrial MBSs and multiple UABSs serve vehicles moving in a city. UAVs can be activated as UABSs to assist vehicles in exchanging data with nearby vehicles. The proposed ILP model jointly optimizes radio resources allocation and beamforming while accounting for vehicular application requirements, backhaul capacity limits, and interference between GUE-UABS and GUE-MBS links. Two system architectures are considered: distributed (MBS-based RRM with shared information) and centralized (network core-based RRM). The percentage of satisfied GUEs has been analyzed and reported a decreasing trend, when getting the requirement on the duration of the service longer. Results showed that deploying UABSs significantly enhances network performance, and the implementation of a centralized architecture with resource sharing has been proven to be the most efficient solution, especially for large values of the MBSs gain. Finally, we have shown that: i) reducing inter-UAV distance increases the maximum $P_g^{(sat)}$, proving that the ILP could handle higher interference levels; ii) a higher number of beams significantly improves performance and iii) higher UABSs activation cost was effective in managing interference, when setting large values of aperture angles at the UABSs.

In future works, we plan to explore the integration of aerial highways, which refer to high-altitude corridors or routes used by aircraft for navigation and air traffic management. These routes are designed to optimize air traffic flow and reduce congestion in the skies. Additionally, we will focus on combining resource allocation with trajectory optimization, through the application of Multi-Agent Deep Reinforcement Learning (MADRL). Through these topics, we aim at advancing the autonomy and adaptability of UAV networks.

Acknowledgment

This work has been carried out in the framework of the CNIT National Laboratory WiLab and the WiLab-Huawei Joint Innovation Center. We would like to thank Aman Jassal for the very fruitful discussion on this paper. Moreover, we would like to express our gratitude to Professor Valentina Cacchiani, from University of Bologna, for her invaluable contribution to the analysis of the complexity of the optimization algorithm presented in the paper.

References

[1] C. Qiu *et al.*, "Joint resource allocation, placement and user association of multiple uav-mounted base stations with in-band wireless backhaul," *IEEE Wireless Communications Letters*, vol. 8, no. 6, pp. 1575–1578, 2019.

[2] O. Bekkouche *et al.*, "Edge cloud resource-aware flight planning for unmanned aerial vehicles," in *2019 IEEE Wireless Communications and Networking Conference (WCNC)*, 2019, pp. 1–7.

[3] O. Andryeyev and A. Mitschele-Thiel, "Efficiency vs. accuracy of aerial base station placement," in *2019 International Conference on Networked Systems (NetSys)*, 2019, pp. 1–8.

[4] H. Yang and X. Xie, "Energy-efficient joint scheduling and resource management for uav-enabled multicell networks," *IEEE Systems Journal*, vol. 14, no. 1, pp. 363–374, 2020.

[5] A. Manzoor, D. H. Kim, and C. S. Hong, "Energy efficient resource allocation in uav-based heterogeneous networks," in *2019 20th Asia-Pacific Network Operations and Management Symposium (APNOMS)*, 2019, pp. 1–4.

[6] Y. Sun *et al.*, "Optimal 3d-trajectory design and resource allocation for solar-powered uav communication systems," *IEEE Transactions on Communications*, vol. 67, no. 6, pp. 4281–4298, 2019.

[7] M. Samir *et al.*, "Trajectory planning and resource allocation of multiple uavs for data delivery in vehicular networks," *IEEE Networking Letters*, vol. 1, no. 3, pp. 107–110, 2019.

[8] N. Namvar *et al.*, "Heterogeneous uav cells: An effective resource allocation scheme for maximum coverage performance," *IEEE Access*, vol. 7, pp. 164 708–164 719, 2019.

[9] M. Chen, W. Saad, and C. Yin, "Liquid state machine learning for resource and cache management in lte-u unmanned aerial vehicle (uav) networks," *IEEE Transactions on Wireless Communications*, vol. 18, no. 3, pp. 1504–1517, 2019.

[10] C. Pan *et al.*, "Joint 3d uav placement and resource allocation in software-defined cellular networks with wireless backhaul," *IEEE Access*, vol. 7, pp. 104 279–104 293, 2019.

[11] L. Deng *et al.*, "Joint resource allocation and trajectory control for uav-enabled vehicular communications," *IEEE Access*, vol. 7, pp. 132 806–132 815, 2019.

[12] J. Ji *et al.*, "Energy consumption minimization in uav-assisted mobile-edge computing systems: Joint resource allocation and trajectory design," *IEEE Internet of Things Journal*, vol. 8, no. 10, pp. 8570–8584, 2021.

[13] Y. Cai *et al.*, "Joint trajectory and resource allocation design for energy-efficient secure uav communication systems," *IEEE Transactions on Communications*, vol. 68, no. 7, pp. 4536–4553, 2020.

[14] F. Zeng *et al.*, "Resource allocation and trajectory optimization for qoe provisioning in energy-efficient uav-enabled wireless networks," *IEEE Transactions on Vehicular Technology*, vol. 69, no. 7, pp. 7634–7647, 2020.

[15] A. Al-Hilo *et al.*, "Uav-assisted content delivery in intelligent transportation systems-joint trajectory planning and cache management," *IEEE Transactions on Intelligent Transportation Systems*, vol. 22, no. 8, pp. 5155–5167, 2021.

[16] M. T. Nguyen and L. B. Le, "Resource allocation, trajectory optimization, and admission control in uav-based wireless networks," *IEEE Networking Letters*, vol. 3, no. 3, pp. 129–132, 2021.

[17] Y. K. Tun *et al.*, "Energy-efficient resource management in uav-assisted mobile edge computing," *IEEE Communications Letters*, vol. 25, no. 1, pp. 249–253, 2021.

[18] T. R. Kamel *et al.*, "Resource allocation in thz unmanned aerial vehicles-based heterogeneous networks," in *2021 International Telecommunications Conference (ITC-Egypt)*, 2021, pp. 1–5.

[19] M. D. Nguyen, L. B. Le, and A. Girard, "Integrated uav trajectory control and resource allocation for uav-based wireless networks with co-channel interference management," *IEEE Internet of Things Journal*, vol. 9, no. 14, pp. 12 754–12 769, 2022.

[20] Y. Xu *et al.*, "Robust resource allocation algorithm for energy-harvesting-based d2d communication underlaying uav-assisted networks," *IEEE Internet of Things Journal*, vol. 8, no. 23, pp. 17 161–17 171, 2021.

[21] Y. Li *et al.*, "Joint resource allocation and trajectory optimization with qos in noma uav networks," in *GLOBECOM 2020 - 2020 IEEE Global Communications Conference*, 2020, pp. 1–5.

[22] Q.-V. Pham *et al.*, "Joint placement, power control, and spectrum allocation for uav wireless backhaul networks," *IEEE Networking Letters*, vol. 3, no. 2, pp. 56–60, 2021.

[23] A. Hajihoseini Gazestani *et al.*, "Resource allocation in full-duplex uav enabled multismall cell networks," *IEEE Transactions on Mobile Computing*, vol. 21, no. 3, pp. 1049–1060, 2022.

[24] Y. Yin *et al.*, "Resource allocation for uav-assisted mimo-noma wireless caching networks," in *2021 IEEE 21st International Conference on Software Quality, Reliability and Security Companion (QRS-C)*, 2021, pp. 1006–1010.

[25] B. Liu *et al.*, "Resource allocation and trajectory design for miso uav-assisted mec networks," *IEEE Transactions on Vehicular Technology*, vol. 71, no. 5, pp. 4933–4948, 2022.

[26] S. Mignardi *et al.*, "Optimizing beam selection and resource allocation in uav-aided vehicular networks," in *2022 Joint European Conference on Networks and Communications & 6G Summit (EuCNC/6G Summit)*, 2022, pp. 184–189.

[27] ETSI, "5G; service requirements for enhanced V2X scenarios," *ETSI TS 22.186 version 16.2.0*, Nov. 2020.

[28] M. H. C. Garcia *et al.*, "A tutorial on 5G NR V2X communications," *IEEE Communications Surveys Tutorials*, pp. 1–1, 2021.

[29] S. Bartoletti *et al.*, "Impact of the generation interval on the performance of sidelink C-V2X autonomous mode," *IEEE Access*, vol. 9, 2021.

[30] ETSI, "Intelligent transport system (ITS); vehicular communications; basic set of applications; analysis of the collective perception service (CPS); release 2," *ETSI TR 103 562 V2.1.1*, 2019.

[31] 5GAA, "C-V2X use cases volume II: Examples and service level requirements," *White Paper*, Jun. 2019.

[32] O. Bouachir *et al.*, "A mobility model for UAV ad hoc network," in *2014 International Conference on Unmanned Aircraft Systems (ICUAS)*, 2014.

[33] 3GPP, "Technical Specification Group Radio Access Network; Study on channel model for frequencies from 0.5 to 100 GHz," *3GPP TR 38.901 version 16.1.0*, Dec. 2019.

[34] ——, "NR overall description," *3GPP TS 38.300*, 2021.

[35] V. K. Salvia, *Antenna and wave propagation*. Laxmi, 2007.

[36] H. Kellerer, "A polynomial time approximation scheme for the multiple knapsack problem," in *International Workshop on Randomization and Approximation Techniques in Computer Science*. Springer, 1999, pp. 51–62.

[37] A. Caprara, H. Kellerer, and U. Pferschy, "The multiple subset sum problem," *SIAM Journal on Optimization*, vol. 11, no. 2, pp. 308–319, 2000.

[38] P. A. Lopez *et al.*, "Microscopic traffic simulation using sumo," in *2018 21st International Conference on Intelligent Transportation Systems (ITSC)*, 2018, pp. 2575–2582.

[39] R. Marini *et al.*, "Reinforcement learning-based trajectory planning for uav-aided vehicular communications," in *2022 30th European Signal Processing Conference (EUSIPCO)*, 2022, pp. 967–971.

[40] L. Spampinato *et al.*, "Drl path planning for uav-aided v2x networks: Comparing discrete to continuous action spaces," in *ICASSP 2023 - 2023 IEEE International Conference on Acoustics, Speech and Signal Processing (ICASSP)*, 2023, pp. 1–5.